The normalized inelastic displacement spectra for seismic response estimation of a SDOF system with a generalized flag-shaped hysteretic model

Yifeng Wu

wuyifeng@bucea.edu.cn

Beijing University of Civil Engineering and Architecture https://orcid.org/0000-0002-6932-2329

Zijian Wang

Beijing University of Civil Engineering and Architecture

Aiqun Li

Beijing University of Civil Engineering and Architecture

Guodong Zhang

Beijing University of Civil Engineering and Architecture

Jiangdi Fu

Beijing University of Civil Engineering and Architecture

Hao Wang

SEU: Southeast University

Research Article

Keywords: Inelastic displacement spectra, Generalized flag-shaped, Normalization, Ductility

Posted Date: June 28th, 2023

DOI: https://doi.org/10.21203/rs.3.rs-3091748/v1

Version of Record: A version of this preprint was published at Bulletin of Earthquake Engineering on March 16th, 2024. See the published version at https://doi.org/10.1007/s10518-024-01886-0.

The normalized inelastic displacement spectra for seismic response estimation of a SDOF system with a generalized flag-shaped hysteretic model

Yifeng Wu[*1] · Zijian Wang[1] · Aiqun Li[1,2] · Guodong Zhang[1] · Jiangdi Fu[1] · Hao Wang[1,2]

Abstract

In order to develop the inelastic displacement spectra suitable for self-centering structures with flag-shaped hysteretic behavior when subjected to near-fault pulse-like (NFPL) ground motions, the nonlinear time history analysis for a single degree of freedom (SDOF) system with a generalized flag-shaped (FS) hysteresis model is first realized by using Matlab software, a total of 85 NFPL records are selected as the seismic input, the variation ranges of all considered parameters, including the ductility, the vibration period, the energy dissipation coefficient and the post-yield stiffness ratio of the hysteresis model are specified, then the constant-ductility inelastic displacement spectra for different seismic records and different parameters are calculated and statistically processed. It is found the normalization of the natural period and the displacement by the pulse period, namely T/T_p and x_m/T_p^2, can significantly reduce the variation of displacement spectra. The influence of the post-yield stiffness ratio ranging from 0 to 0.20 on the normalized spectra is slight and can be neglected. Besides, as T/T_p increases, the normalized displacement first increases and then slowly decreases, the normalized period corresponding to the peak displacement is approximately 1. When T/T_p is about less than 0.7, the displacement spectra are positively correlated with the ductility, μ, followed by a negative correlation between them as T/T_p grows larger. Moreover, increasing the energy dissipation coefficient will reduce the displacement response, but when the coefficient is greater than 1, its impact on the displacement is rather small. Finally, the equation of the normalized displacement spectra as a function of T/T_p and μ is proposed, and an adjustment factor is added to account for the influence of the energy dissipation coefficient on the displacement spectra.

Keywords Inelastic displacement spectra · Generalized flag-shaped · Normalization · Ductility · Energy dissipation coefficient · Fitting formula

1. Introduction

With the rapid development of society and the continuous advancement of urbanization, the huge economic loss caused by earthquake disasters arises public's wide concern. For example, there is

* Yifeng Wu

wuyifeng@bucea.edu.cn

[1] School of Civil and Transportation Engineering, Beijing University of Civil Engineering and Architecture, Beijing 100044, China

[2] School of Civil Engineering, Southeast University, Nanjing 210096.

more than 30 billion dollars loss in Northridge earthquake (1994) and up to 100 billion dollars in Wenchuan earthquake (2008). In order to effectively control structural damage and reduce the post-earthquake repair costs, a performance-based seismic design concept was proposed in the 1990s (Fajfar and Krawinkler 1997), numerous researches on this topic were then reported in the last 30 years (Priestley 2000). Since the performance and damage level of structures are closely related to deformation, and the displacement is much easier to be understood and calculated compared with other indicators, such as energy (Dindar et al. 2015) and damage (Bozorgnia and Bertero 2003; Wen et al. 2014), the displacement based seismic design method is currently the most acceptable, in which obtaining the displacement response spectra is very crucial.

According to whether the nonlinear behavior of structures is considered under earthquake action, the response spectra can be divided into elastic and inelastic ones. The elastic response spectra were developed in the early 1930s and have been extensively applied in structural design. In recent decade, Bommer et al. (1999) presented elastic displacement spectra applicable for various soil sites with magnitude between 5.5 and 7.5, epicentral distance less than 50km and damping ratio ranging from 5% to 30%. Akkar et al. (2007) pointed out the underestimation of spectra ordinates at longer periods due to severe filtering. Bommer et al. (2004) expanded the period range of the spectra to 10s, and Chih-Hsuan Sung.et al. (2021) took the permanent tectonic displacement into consideration. However, structures probably experience nonlinear behavior when strong earthquake occurs, in such case it is more reasonable to develop inelastic displacement spectra to estimate the maximum deformation (Chopra and Goel 2001; Mavroeidis et al. 2004). At present, most of the researches corresponding to inelastic displacement spectra mainly focus on the strength reduction factor, R, or the inelastic displacement ratio, C. Their influential factors including site soil conditions (Miranda 2000; Ruiz-García and Miranda 2004), earthquake characteristics (Mavroeidis et al. 2004; Gillie et al. 2010; Iervolino et al. 2012; Ruiz-García 2011; Durucan and Dicleli 2015), hysteresis models (Chenouda and Ayoub 2008; Song and Gavin 2011; Song et al. 2014) and soil structure interaction (Khoshnoudian and Ahmadi 2015; Demirol and Ayoub 2017) are totally investigated. A few other studies (Tothong and Cornell 2006; Stafford et al. 2016; Heresi et al. 2018) utilized an alternative method to assess the direct inelastic spectral displacement demand rather than the above intermediate variables, R and C, among which the inelastic displacement as a function of magnitude, epicenter distance, structural period and yield strength coefficient was presented by Stafford et al. (2016) for four common hysteretic models. Wu et al. (2019) established the inelastic spectra of SDOF systems with high ductility being up to 70, and the direct displacement-based seismic design method using the spectra for a continuous seismic isolated beam bridge was demonstrated.

On the other hand, more and more studies focused on the self-centering structures recently, this type of structures have distinct characteristics of stable energy dissipation and small residual deformation, which can significantly improve structural seismic resilience and reduce the repair costs. The flag-shaped (FS) hysteresis model is typically used to characterize the force-displacement hysteretic relations of these structures (Eatherton et al. 2014; Zhu and Zhang 2007; Xu et al. 2023). For this hysteresis model, Francesco et al. (2019) conducted a statistical research on inelastic displacement ratio with large variability of vibration periods, ductility, and post-yield stiffness ratios. Dong et al. (2020) and Zhu Ruizhao et al. (2022) respectively compared the inelastic displacement ratio calculated from near-fault pulse-like (NFPL) ground motions and far-fault ones, and found that

the long period pulse will result in a higher deformation demand for structures.

In summary, a lot of efforts have been made to assess the inelastic displacement response of SDOF systems with different hysteresis models, and the effects of NFPL records are comprehensively explored in the past few decades. However, the direct estimation of the maximum inelastic displacement for the FS hysteresis models, rather than relating it to elastic displacement by the aforementioned C or R, is still limited. In addition, due to the strong randomness of ground motions, it is necessary to reduce the dispersion of the displacement response. Therefore, the main objective of this article is to develop the normalized inelastic displacement spectra with less dispersion for self-centering structures exhibiting flag-shaped hysteretic behavior when subjected to NFPL ground motions. We first implement the nonlinear time history analysis for SDOF systems with generalized flag-shaped (FS) hysteresis models in Matlab, the validity of the normalization method to reduce the variation of results is then evaluated. Afterwards the influences of the ductility, the structural period, the energy dissipation coefficient and the post-yield stiffness ratio of the hysteresis model on the normalized spectra are analyzed statistically. Furthermore, a fitting formula for the spectra is established for practical use in displacement-based seismic design of self-centering structures.

2. Ground motion database

For NFPL ground motions, the extraction and recognition of the long-period pulses is essential (Chang et al. 2016). Based on the continuous wavelet transform, Baker et al. (2007) extracted the strongest pulse from the velocity time history curve, and the corresponding pulse period T_p was subsequently determined. Shahi et al. (2014) improved this method by synthesizing orthogonal bidirectional seismic records to directly determine the orientation with the strongest pulse and extract it. In this study, a total of 85 NFPL records with rupture distance (Rrup) less than 20km from 32 earthquake events are selected from the NGA-West2 ground motion database. The detailed information of each record, such as magnitude (M_w), rupture distance, peak ground velocity (PGV), and T_p, is presented in Table 1.

Table 1 NFPL records used in this study

Earthquake (Year)	Station	M_w	R_{rup} (km)	PGV (cm/s)	T_p (s)
San Fernand (1971)	Pacoima Dam (upper left abut)	6.6	1.8	121.9	1.64
Coyote Lake (1979)	Gilroy Array #2	5.7	9	32	1.46
	Gilroy Array #4		5.7	32.1	1.35
	Gilroy Array #6		3.1	49.6	1.23
Imperial Valley-06(1979)	Agrarias	6.5	0.7	53.5	2.34
	Brawley Airport		10.4	36.7	4.4
	EC County Center FF		7.3	70.8	4.42
	El Centro-Meloland Geot. Array		0.1	116.4	3.42

Earthquake (Year)	Station	M_w	R_{rup} (km)	PGV (cm/s)	T_p (s)
Imperial Valley-06(1979)	El Centro Array #10	6.5	8.6	55.2	4.52
	El Centro Array #3		12.9	55.8	4.5
	El Centro Array #4		7	80.8	4.79
	El Centro Array #5		4	96.5	4.13
	El Centro Array #6		1.4	121.6	3.77
	El Centro Array #7		0.6	111.9	4.38
Mammoth Lakes-06 (1980)	Holtville Post Office	5.9	7.5	73.4	4.82
	Long Valley Dam (Upr L Abut)		16	43.3	1.01
Westmorland (1981)	Parachute Test Site	5.9	16.7	60.8	4.39
	Westmorland Fire Sta		6.5	52.9	1.22
Morgan Hill(1984)	Coyote Lake Dam (SW Abut)	6.2	0.5	76.8	1.07
	Gilroy Array #6		9.9	37.3	1.23
N. Palm Springs (1986)	Morongo Valley Fire Station	6.1	12	39.4	2.38
San Salvador(1986)	National Geografical Inst	5.8	7	92.2	1.13
Superstition Hills-02 (1987)	Kornbloom Road (temp)	6.5	18.5	33.1	2.13
	Parachute Test Site		0.9	143.9	2.39
Loma Prieta (1989)	Poe Road (temp)	6.9	11.2	42.1	2.87
	Gilroy - Historic Bldg.		11	43.6	1.64
	Gilroy Array #2		11.1	46.2	1.73
	Gilroy Array #3		12.8	44.8	2.64
	Saratoga - Aloha Ave		8.5	53.5	4.57
	Saratoga - W Valley Coll.		9.3	62	5.65
Cape Mendocino (1992)	Cape Mendocino	7	7	124.1	4.84
	Petrolia		8.2	96.7	3
Landers (1992)	Lucerne	7.3	2.2	132.3	5.12
Northridge-01 (1994)	Jensen Filter Plant	6.7	5.4	101.5	3.16
	Jensen Filter Plant Generator		5.4	66.1	3.54
	LA Dam		5.9	86.3	1.62
	Newhall - Fire Sta		5.9	116.1	1.37
	Newhall - W Pico Canyon Rd.		5.5	118.3	2.98
	Rinaldi Receiving Sta		6.5	149.1	1.25
	Sylmar - Converter Sta		5.3	106.3	2.98
	Sylmar - Converter Sta East		5.2	114	3.53
	Sylmar - Olive View Med FF		5.3	130.6	2.44
Kobe, Japan (1995)	KJMA	6.9	1	105.6	1.09
	Port Island (0 m)		3.3	103	2.83
	Takarazuka		0.3	95.6	1.81
	Takatori		1.5	153.2	1.55
Kocaeli, Turkey (1999)	Gebze	7.5	10.9	53	5.99
	Izmit		7.2	38.1	5.37
	Yarimca		4.8	90.6	4.95
Chi-Chi, Taiwan (1999)	CHY101	7.6	9.9	108.9	5.34
	TCU036		19.8	63.2	5.38
	TCU065		0.6	136.5	5.74
	TCU075		0.9	104.9	5
	TCU076		2.7	71.2	4.73

Earthquake (Year)	Station	M_w	R_{rup} (km)	PGV (cm/s)	T_p (s)
Duzce, Turkey(1999)	Duzce	7.1	6.6	78.9	5.94
Northwest China -03(1997)	Jiashi	6.1	17.7	34.6	1.09
Denali, Alaska (2002)	TAPS Pump Station #10	7.9	2.7	121.4	3.16
Chi-Chi, Taiwan-03 (1999)	CHY024	6.2	19.6	32.7	3.19
Chi-Chi, Taiwan-03 (1999)	TCU078		7.6	56.3	3.86
Chi-Chi,Taiwan-04(1999)	CHY074	6.2	6.2	44	2.44
Chi-Chi,Taiwan-06(1999)	TCU078	6.3	11.5	38.4	4.15
Loma Prieta (1989)	Los Gatos-Lexington Dam	6.9	5	121.3	1.57
Cape Mendocino	Bunker Hill FAA	7	12.2	80.6	5.36
(1992)	Centerville Beach		18.3	57.5	1.97
Tottori, Japan (2000)	TTR008	6.6	6.9	53.2	1.54
Parkfield-02, CA	PARKFIELD - EADES	6	2.9	35.8	1.22
(2004)	Parkfield - Cholame 2WA		3	57.9	1.08
	Parkfield - Fault Zone 1		2.5	81.9	1.19
	Parkfield - Fault Zone 12		2.6	56.5	1.19
Montenegro, Yugo.	Bar-Skupstina Opstine	7.1	7	62.7	1.44
(1979).	Ulcinj - Hotel Olimpic		5.8	62.8	1.97
L'Aquila, Italy	L'Aquila- Centro Valle	6.3	6.3	42.1	1.07
(2009)	L'Aquila -F. Aterno		6.5	31.6	1.18
Chuetsu-oki	Joetsu Kakizakiku	6.8	11.9	91.1	1.4
(2007)	Yoshikawaku Joetsu City		16.9	63.8	1.33
	Kashiwazaki City Center		11.1	126	2.93
	Kariwa		12	154.5	3.08
	Yan Sakuramachi City watershed		19	39.4	1.41
Iwate (2008)	IWTH26	6.9	6	56.9	4
Christchurch, New Zealand	CCCC	6.1	3.3	66.9	1.72
(2011)	CHHC		4.8	81.3	1.96
	CMHS		4.5	48.1	2.04
	PRPC		2	123.1	4.82
	REHS		5.1	97.5	1.55
	SHLC		5.6	72.4	3.58

3. Methodology

3.1 The motion equation of SDOF systems

This article utilizes the incremental form of the governing motion equation of SDOF systems as shown in Eq. (1), and solves it by the Newmark implicit time integration method. The implementation of the analysis is carried out in Matlab,

$$m\Delta\ddot{x}(t) + c\Delta\dot{x}(t) + k\Delta x(t) = -m\Delta\ddot{x}_g(t) \tag{1}$$

in which m is the system mass, c is the linear viscous damping, k is the instantaneous stiffness varying with time and determined by the FS hysteresis. $\Delta\ddot{x}(t)$, $\Delta\dot{x}(t)$ and $\Delta x(t)$ are respectively the increments of acceleration, velocity and displacement of the system. $\Delta\ddot{x}_g(t)$ is the increment of the earthquake acceleration.

3.2 The ductility ratio μ

μ is the displacement ductility reflecting the inelastic deformation ability of structures, it is defined by the ratio of the maximum absolute displacement to the yield displacement of the system,

$$\mu = \frac{x_m}{x_y} \tag{2}$$

where x_m is the maximum displacement, x_y is the displacement corresponding to the yielding restoring force, F_y. The ductility ratio is usually less than 8 for conventional structures, and six values of constant ductility ratio ranging from 1 to 6 with equal interval are utilized in this study.

3.3 Parameters of the FS hysteresis model

The energy dissipation coefficient, β, is a key parameter of the FS hysteresis model, it is determined by the ratio of the energy dissipation area of the model to that of the bilinear elasto-plastic model with the same maximum displacement. In this study, β varies from 0 to 2 with an increment of 0.25 to enhance its generality. The FS model will be attenuated and exhibit bilinear-elastic behavior when β equals to 0, and it will change to the bilinear elasto-plastic model when β is 2. Fig. 1 shows the hysteretic model where β respectively equals to 0.5 and 1.5. It is obvious the influence of β on the inelastic displacement spectra cannot be neglected (Stafford et al. 2016; Stafford et al. 2019). Additionally, the post-yield stiffness ratio, α, is the ratio of the post-yield stiffness to the pre-yield stiffness, it is set as 0 0.05, 0.10, 0.15, 0.20 in this study (Wu et al. 2019; Dong et al. 2020).

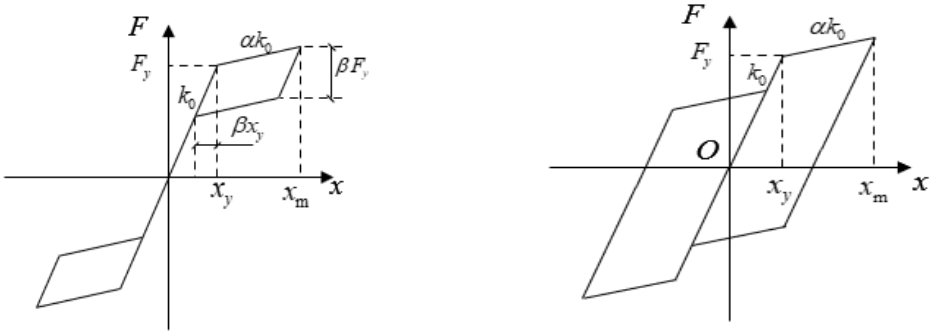

(a) β=0.5 (b) β=1.5

Fig. 1 Influence of β on the FS model

3.4 Calculation procedure

The following procedure illustrated in Fig. 2 is employed to calculate the maximum inelastic displacement, x_m. The period, T, of the SDOF system ranges from 0.05s to 20s with an increment of 0.05s. The inherent elastic damping ratio is 5%. The kernel of the procedure is the iterative nonlinear time history analyses before convergence. For a target ductility, μ_0, the yield displacement, x_y, of the SDOF system cannot be determined in advance and an assumed x_y is needed. Taking the period of 0.5s as an example, the assumed x_y is initialized by the final convergent x_y of the previous

closest period, namely 0.45s as the period increment is 0.05s. The assumed x_y for the first period 0.05s is 0.001m. After all parameters are specified, the nonlinear time history analysis is performed, the maximum displacement as well as the actual computed μ can be obtained. If the error between μ and μ_0 is larger than a tiny number, ε, 2% in this study, x_y will be re-assumed by x_m/μ_0 and a next iteration analysis is followed. In certain circumstances of the iteration steps larger than 3, x_y of the next iteration is determined by the average of that in the last two iterations to avoid numerical oscillation.

In order to demonstrate the computation process of the procedure, taking the Takatori record of Kobe earthquake in 1995 as an example, the target ductility μ_0=4, T=0.9s and β=0.5, a total of eight iterations of analyses are performed according to the calculation procedure. The displacement time history of the 1st, 5th and 8th iteration is presented in Fig. 3, from which we can see the assumed x_y has a direct impact on the displacement response of the SDOF system. The hysteresis curve of the final iteration is shown in Fig. 4.

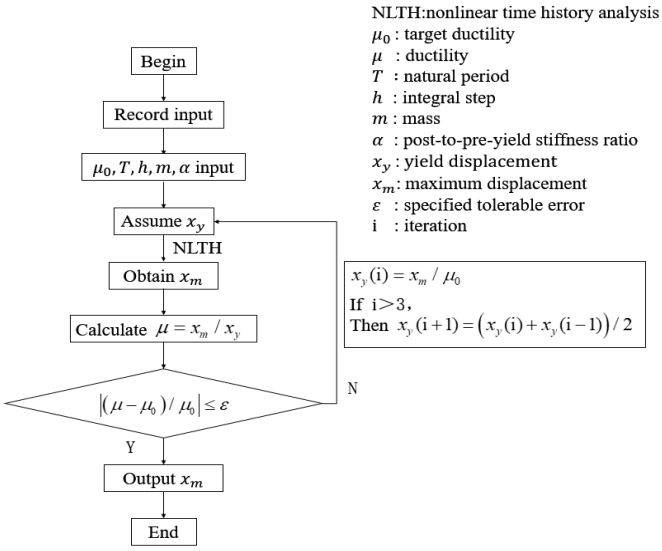

Fig. 2 Flowchart of the calculation procedure for the inelastic displacement spectra.

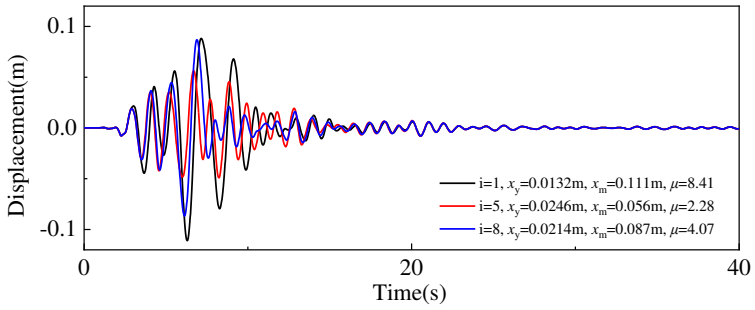

Fig. 3 Program running example

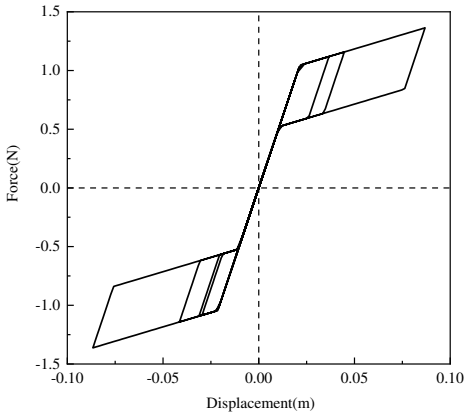

Fig. 4 Hysteresis curve example

In the above example, the peak ground acceleration (PGA) of each seismic record has been modified to 1m/s^2. If it is set as 10m/s^2, the displacement response of the 8th iteration drawn with solid black line in Fig. 5 is exactly 10 times of the original one with solid red line. Actually, for a constant ductility, μ_0, the maximum inelastic displacement is linearly related to the peak ground acceleration (Sucuoğlu et al. 1994), so only one set of PGA value needs to be considered. In this study, it is set as 1m/s^2 for all records.

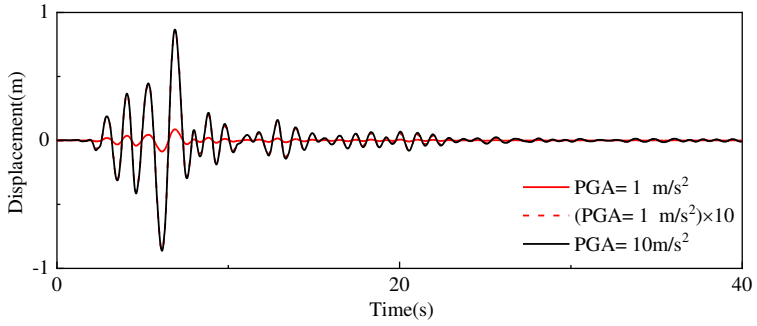

Fig. 5 The displacement response with different PGA values

3.5 Normalization of the spectra

Due to strong randomness of seismic records, there are significant differences in their spectral characteristics, and the resulting dispersion in the inelastic spectra is sometimes unacceptable. In view of this, the pulse period, the predominant period, the ratio of V_p/A_p and some other parameters were utilized to normalize the system period in several studies (Mavroeidis et al. 2004; Gillie et al. 2010; Iervolino et al. 2012; Ruiz-García 2011; Durucan and Dicleli 2015) to reduce the dispersion of R and C, and the first one was found to have the best effect for NFPL ground motions. This method is also suitable for the inelastic displacement spectra, but the difference is that R and C are dimensionless variables, while the maximum displacement is not. Therefore, apart from the above mentioned T/T_p, the obtained x_m should also be normalized by T_p^2 according to the following equation (Wu et al. 2019),

$$x_m / T_p^{\,2} = C \left(\frac{T / T_p}{2\pi} \right)^2 A \tag{3}$$

where A is the design elastic pseudo acceleration.

The following is an example to illustrate the effect of normalization, in which the stiffness ratio,

α, is taken as 0.1, the energy dissipation coefficient, β, is 0.5. The mean inelastic displacement spectra before and after normalization are shown in Fig. 6. Since the maximum pulse period is 6s in Tab. 1, the normalized dimensionless variable, T/T_p, ranges from 0 to 3 for simplicity (Iervolino et al. 2012; Ruiz-García 2011). In general, the variation of x_m/T_p^2 with respect to the period and ductility is relatively similar to that before normalization. In addition to the mean results, the coefficient of variation (COV) of the displacement spectra with respect to T and T/T_p are presented in Fig. 6. Here COV is computed by dividing the standard deviation by the mean to assess the dispersion, which is also a dimensionless variable. Obviously, it increases rapidly at first and then varies little in the long period range, while it is almost independent on the ductility level over the whole range. Besides, it can be concluded that the scatter of x_m/T_p^2 is effectively reduced compared with that of the spectra before normalization. So, all the subsequent analyses are based on the normalized results.

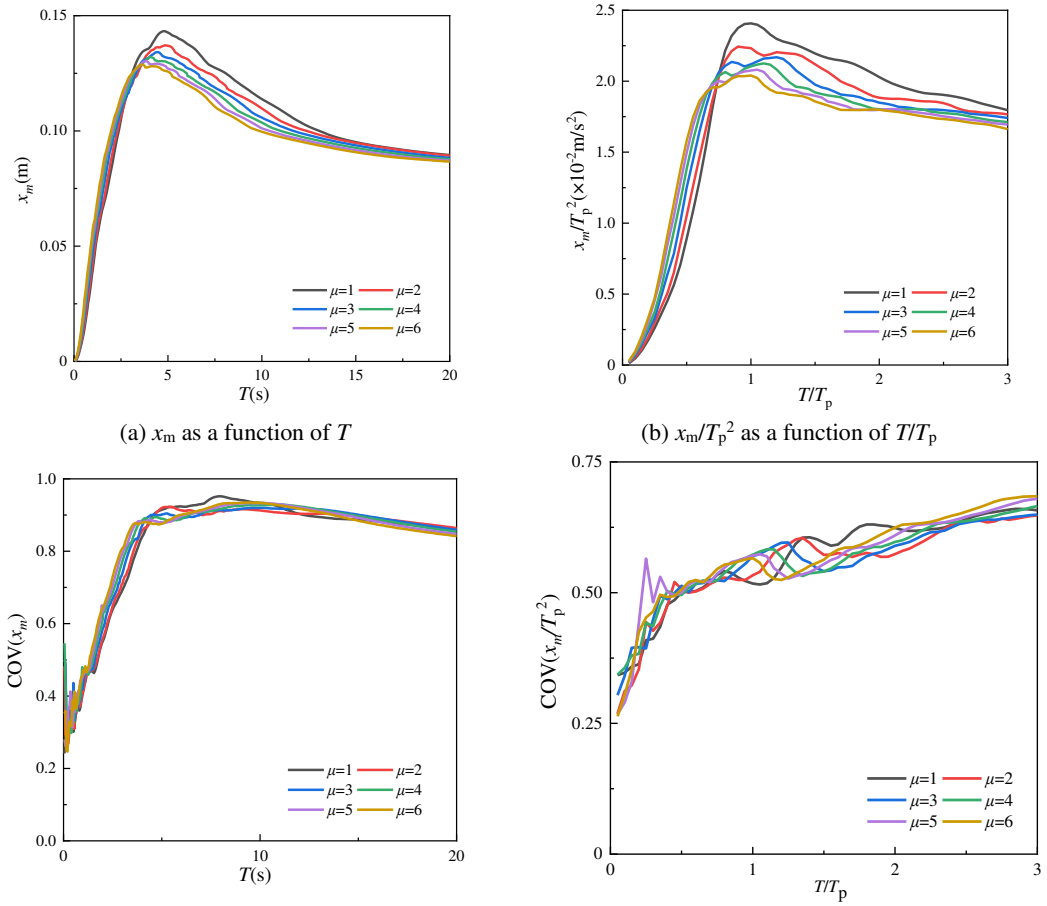

(a) x_m as a function of T

(b) x_m/T_p^2 as a function of T/T_p

(c) COV of x_m as a function of T

(d) COV of x_m/T_p^2 as a function of T/T_p

Fig. 6 The effects of normalization on the inelastic displacement spectra

4. The influential factors on the normalized spectra

4.1 The post-yield stiffness ratio α

The self-centering structures can be designed to have variable post-yield properties. In order to study the effects of α on the maximum displacement response, the mean normalized displacement spectra of all the 85 NF pulse-like records are computed respectively with the ratio being 0, 0.05, 0.1, 0.15 and 0.2. Due to similar features and limited space, only the results in the four cases (μ=2, 5; β=0.5,

1.5) are illustrated in Fig. 7. It is not difficult to find that the effects of the post-yield stiffness ratio ranging from 0 to 0.2 on the displacement spectra is rather small and can be neglected, and the ratio is uniformly set to 0.1 in subsequent studies.

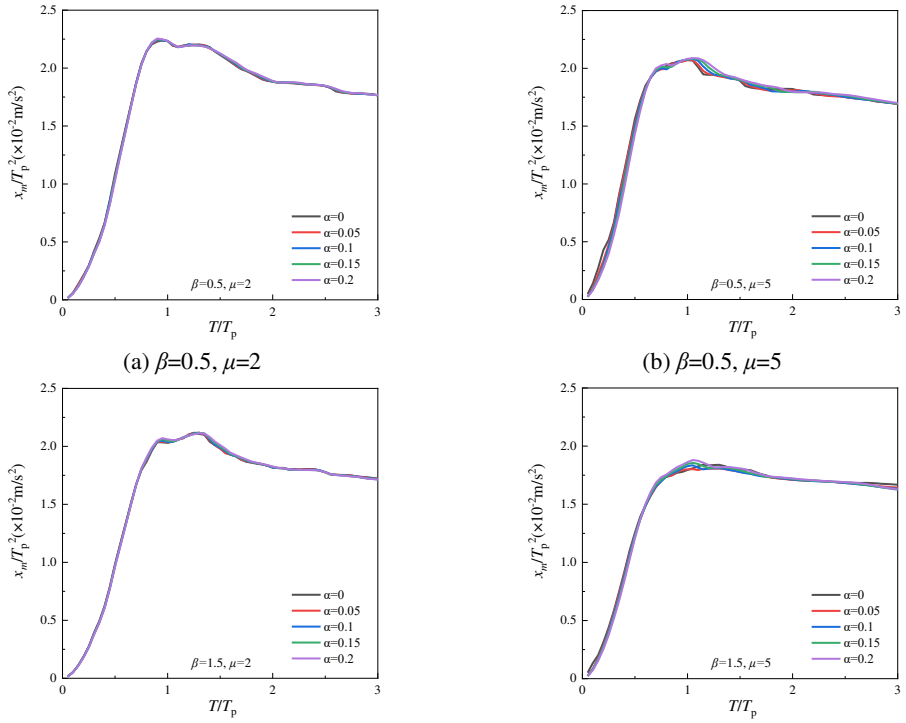

(a) β=0.5, μ=2 (b) β=0.5, μ=5

(c) β=1.5, μ=2 (d) β=1.5, μ=5

Fig. 7 Effect of the stiffness ratio on normalized displacement spectra with different parameters

4.2 The ductility level μ

Taking the energy dissipation coefficient equaling to 0.25, 1.0 and 1.75 as the representative of low, medium and high energy dissipation capacity, the normalized spectra with the ductility level ranging from 1 to 6 are illustrated in Fig. 8. It is observed the ordinates x_m/T_p^2 first increases and then slowly decreases, the normalized period corresponding to the peak value of each curve is approximately 1, the peak value varies from 1 0.0175m/s^2 to 0.025m/s^2 for different μ and β given PGA being 1m/s^2 in this study, and the last value of for all curves is about 0.017m/s^2. When T/T_p is approximately less than 0.7, x_m/T_p^2 is positively correlated with the ductility level, followed by a negative correlation between them as T/T_p grows larger. For this reason, a small intersection area marked by a circle is shown in each subfigure. Moreover, the displacement spectra are less affected by the ductility when it is greater than 4.

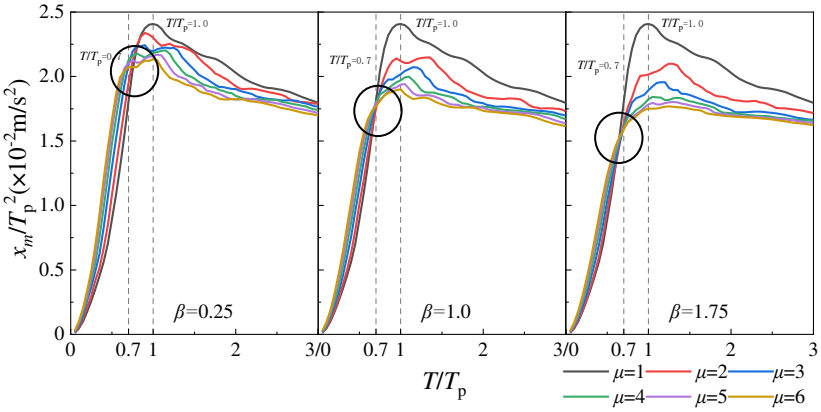

Fig.8 Influence of the ductility on the normalized displacement spectra

4.3 The energy dissipation coefficient β

The coefficient β of the FS model can be designed by changing the mechanical and dimension parameters of the energy dissipation devices in self-centering structures. It has no impact on the elastic displacement spectra as μ equals to 1. Fig. 9 shows the influence of β on the inelastic spectra when μ=2, 4, and 6, which represents the results for low, moderate and high ductility levels. Obviously, the spectral value gradually decreases with the increase of β. From the perspective of energy, the larger β means the higher energy dissipation ability of the structure, and a resulting lower mean displacement response is reasonable. However, it can also be found that the reduction rate grows smaller as β increases, especially when β is greater than 1, its influence on the spectra is rather small and can even be ignored.

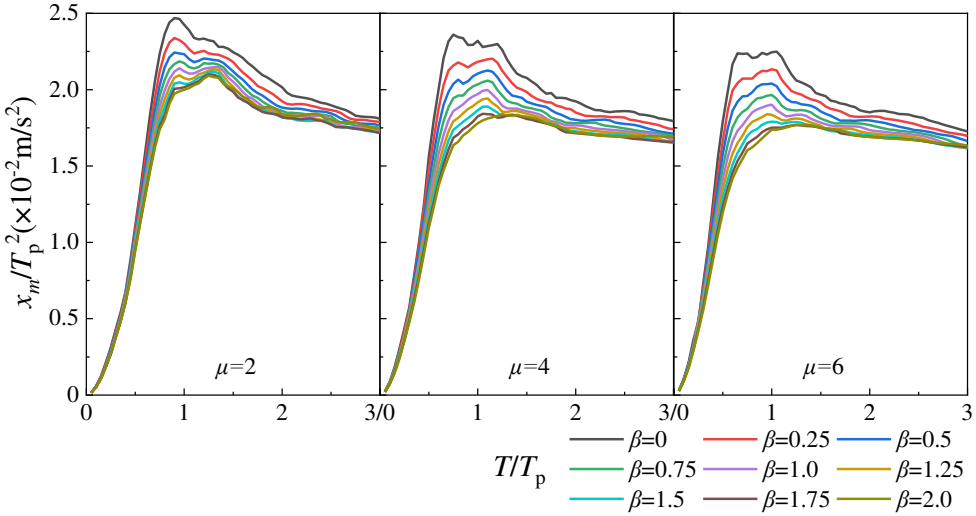

Fig. 9 Influence of the energy dissipation coefficient on the normalized displacement spectra

In view of the similar variation trend of the curves in Fig. 9, the range of β are further divided into the two intervals, namely [0-1] and [1-2]. To quantify the differences introduced by the energy dissipation coefficient, the ratio, Ω_β, based on the displacement spectra with different β values is defined as follows.

$$\Omega_\beta=\begin{cases} x_{\mathrm{m},\beta}/x_{\mathrm{m},0.5} & (\beta=0,\ 0.25,\ 0.5,\ 0.75,\ 1) \\ x_{\mathrm{m},\beta}/x_{\mathrm{m},1.5} & (\beta=1,\ 1.25,\ 1.5,\ 1.75,\ 2) \end{cases} \tag{4}$$

in which $x_{\mathrm{m},\beta}$ is determined by the normalized spectra in Fig. 9. This equation takes the results of β=0.5 and 1.5 as references, and Ω_β is an indicator to measure the difference introduced by β in the above two intervals.

According to Eq. (4), the variation of Ω_β with respect to T/T_p is illustrated in Fig. 10. It is clearly shown that Ω_β varies in the range between 0.9 and 1.1 in most cases, especially when T/T_p is larger than 1, the value of all curves slowly tends to 1, indicating the slighter effects of β on the displacement spectra. In order to simplify considering the effects of β, the mean value of Ω_β is also drawn in Fig. 10 with dashed line, from which we can see the error introduced by averaging Ω_β irrespective of the variation of T/T_p is insignificant.

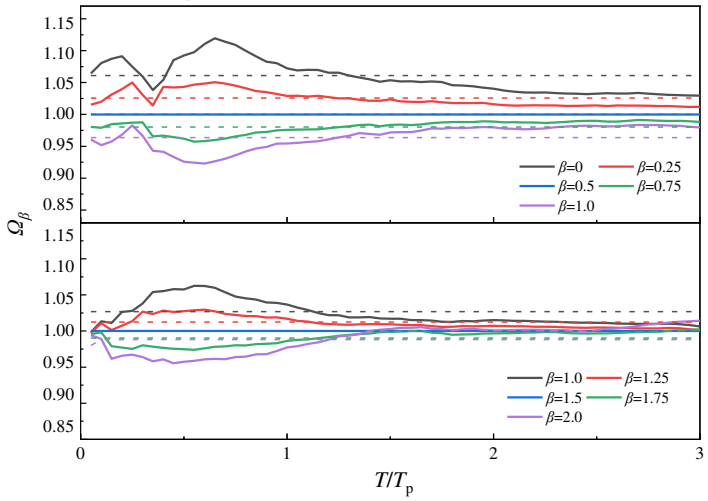

Fig.10 Impact of energy consumption coefficient on the normalized displacement spectra

The detailed mean values of Ω_β are given in Table 2. Given the same T/T_p and μ, the maximum inelastic displacement for any β, 0 for example, is simplified by multiplying that of β=0.5 with the mean value 1.06. For other values of β not in Table 2, Ω_β is determined by linear interpolation method, that is to say the value of Ω_β for β=0.9 and 1.1 is respectively about 0.97 and 1.02.

Table 2 Mean of Ω_β

β	0	0.25	0.5	0.75	1.0	1.25	1.5	1.75	2.0
Ω_β	1.06	1.03	1	0.98	0.96/1.03	1.01	1	0.99	0.99

5. Fitting formula for the normalized inelastic displacement spectra

To facilitate the use of the displacement spectra as presented in Fig. 8 and Fig. 9, it is desirable to have a mathematical fitting formula for the spectra. Since the effect of β has been quantified in Table 2, only the normalized period and ductility level need to be included in the formula. After analyzing the variation of $x_\mathrm{m}/T_\mathrm{p}^2$ in the above figures, a comprehensive equation, including three undetermined functions of f, g, k and PGA, is proposed as follows (Wu et al. 2019),

$$x_m / T_p^{\,2} = f \cdot \mathrm{g} \cdot k \cdot (\mathrm{PGA}) \cdot \Omega_\beta \tag{5}$$

$$f(T/T_\mathrm{p}, \mu) = \exp\left(p1 \cdot (T/T_\mathrm{p})^3 + p2 \cdot (T/T_\mathrm{p})^2 + p3 \cdot \mu^2 + p4 \cdot (T/T_\mathrm{p}) \cdot \mu + p5 \cdot (T/T_\mathrm{p}) + p6 \cdot \mu + p7 \right) \tag{6}$$

$$g(T/T_\mathrm{p}, \mu) = (T/T_\mathrm{p})^{g1 \cdot \mu^{g2}} \tag{7}$$

$$k(T/T_\mathrm{p}, \mu) = \mu^{k1 (T/T_\mathrm{p})^{k2}} \tag{8}$$

where f utilizes exponential function to ensure positive, and a cubic polynomial equation accounting for the effects of μ and T/T_p on the normalized displacement spectra is employed as the exponential coefficient. Besides, two symmetrical power functions, g and k, are added to better characterize the features of $x_\mathrm{m}/T_\mathrm{p}^2$. As mentioned above, the normalized displacement response is linearly correlated with PGA, so the multiplication of PGA is also needed in Eq. (5). Besides, $p1$ to $p7$ and $g1$, $g2$, $k1$, $k2$ are the undetermined parameters. According to the spectral results of β=0.5 and 1.5, as well as those of μ=1, all the parameters shown in Table 3 are obtained by nonlinear regression analyses using the Levenberg–Marquardt algorithm (Marquardt 1963).

Table 3 The identified parameters

	p1	*p2*	*p3*	*p4*	*p5*	*p6*	*p7*	*g1*	*g2*	*k1*	*k2*	Correlation coefficient
μ=1	-0.341	3.04	1.36	-9.35	-2.25	2.00	1.79	6.78	3.14	0	0	0.997
β=0.5	-0.318	2.73	0.0188	0.0448	-10.2	-0.352	4.14	6.01	0.00399	0.550	-0.746	0.997
β=1.5	-0.239	2.13	0.0189	0.0343	-8.32	-0.333	2.73	5.14	0.0141	0.455	-0.764	0.998

Fig. 11 illustrates part of the fitting results according to Eq. (5), which is the counterpart of those in Fig. 9, from which we can see the variation features of the normalized spectra are well captured. The correlation coefficients are respectively 0.997, 0.997 and 0.998, indicating a high degree of fit using the above equation and identified parameters. Moreover, the error between the fitting and the original spectra is presented in Fig. 12, where it is lower than 0.001m/s^2 in most cases of T/T_p, μ and β. Only when β equals to 0, actually impossible for self-centering structures, the error reaches up to 0.002m/s^2 in a small range of T/T_p. To conclude, the proposed equations and the identified parameters in Table 3 are capable of reproducing the normalized displacement spectra very well.

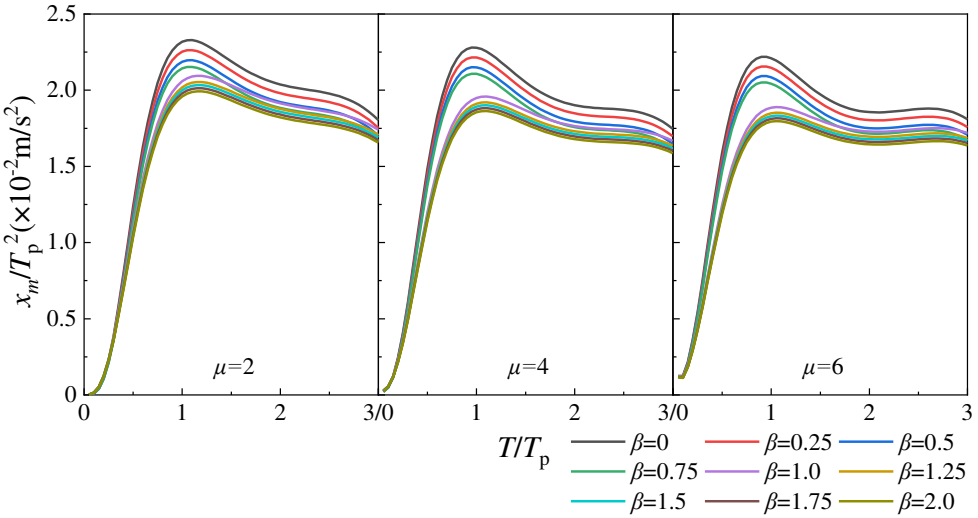

Fig.11 Fitting for the normalized inelastic displacement spectra

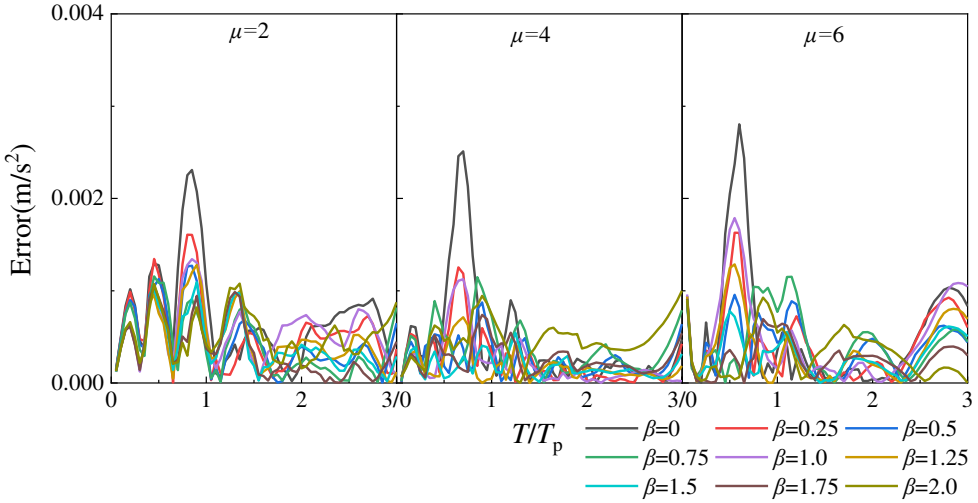

Fig.12 Error on the normalized displacement spectra

It should be noted the complete procedures to get the normalized inelastic displacement spectra are presented in this study, including arranging a pool of particular ground motions, calculating the normalized x_m/T_p^2 of each record, statistically analyzing the results, proposing the fitting equations and conducting nonlinear regression analyses. The whole work is based on the 85 records in Table 1, for other different groups of records, the corresponding spectra are probably similar to those in this study, and can also be developed according to the same procedures. Besides, for the estimation of T_p as a function of magnitude or other earthquake parameters, it can be accessed in some other researches (Mavroeidis et al. 2004; Gillie et al. 2010; Durucan and Dicleli 2015) and is not included in this study.

6. Conclusions

This article focuses on the inelastic displacement spectra suitable for the self-centering structures characterized by FS hysteresis model when subjected to NFPL ground motions. The pulse period is utilized to normalize the structural period and maximum inelastic displacement. Then the effects of the post-stiffness ratio, ductility level as well the energy dissipation coefficient on the displacement

spectra are quantitatively investigated. The main conclusions obtained are as follows.

(1) The scatter of the spectra before normalization is strong over the whole period range due to the randomness of the earthquake characteristics, but it can be significantly reduced by the normalization of T/T_p and x_m/T_p^2.

(2) As the post-stiffness ratio varies in the range between 0 and 0.2, it has little impact on the normalized displacement spectra.

(3) With the increasing of T/T_p, all the normalized displacement spectra values with different influential parameters first increase rapidly and then slowly decrease, tending to 0.017m/s^2 in the end. Besides, the value of T/T_p corresponding to the maximum ordinate is approximately 1 in almost all cases.

(4) In the short normalized period range, about less than 0.7, the normalized displacement spectra are positively correlated with the ductility. However, negative correlation between them is found as the normalized period grows larger.

(5) The inelastic displacement spectra will be reduced with the increase of energy dissipation coefficient. However, when the coefficient is larger than 1, its influence on the spectra is rather small.

(6) The proposed fitting formula and the identified parameters, as well as the adjustment factor, proves efficient to characterize the complex variation of x_{max}/T_p^2. It is advisable to use Eq. (5) to estimate the maximum displacement response of FS hysteresis model with different design parameters when subjected to NFPL ground motions.

Funding The authors would like to gratefully acknowledge the financial support for this research provided by the R&D Program of Beijing Municipal Commission of Education [No. KM202310016012], National Natural Science Foundation of China [No. 51908024], the Pyramid Talents Development Project-Outstanding Scholar of BUCEA [No. JDYC20200310]

Conflict of interest The authors declare that they have no known competing financial interests or personal relationships that could have appeared to influence the work reported in this paper.

References

Akkar S, Bommer JJ (2007) Prediction of elastic displacement response spectra in Europe and the Middle East. Earthq Eng Struct D, 36(10): 1275-1301.https://doi.org/10.1002/eqe.679

Baker JW (2007) Quantitative classification of near-fault ground motions using wavelet analysis. B Seismol Soc Am, 97(5): 1486-1501.https://doi.org/10.1785/0120060255

Bommer JJ, Elnashai AS (1999) Displacement spectra for seismic design. J Earthq Eng, 3(01): 1-32.https://doi.org/10.1080/13632469909350338

Bozorgnia Y, Bertero VV (2003) Damage spectra: Characteristics and applications to seismic risk reduction. J Struct Eng, 129(10): 1330-1340.https://doi.org/10.1061/(ASCE)0733-9445(2003)129:10(1330)

Chang ZW, Sun XD, Zhai CH, Zhao JX, Xie LL (2016) An improved energy-based approach for selecting pulse-like ground motions. Earthq Eng Struct D, 45 (14): 2405-2411.https://doi.org/10.1002/eqe.2758

Chenouda M, Ayoub A (2008) Inelastic displacement ratios of degrading systems. J Struct Eng, 134(6): 1030-1045.https://doi.org/10.1061/(ASCE)0733-9445(2008)134:6(1030)

Chopra AK, Goel RK (2001) Direct displacement-based design: use of inelastic vs. elastic design spectra. EARTHQ SPECTRA, 17(1): 47-64.https://doi.org/10.1193/1.1586166

De Francesco G (2019) Constant-ductility inelastic displacement ratios for displacement-based seismic design of self-centering structures. Earthq Eng Struct D, 48(2): 188-209.https://doi.org/10.1002/eqe.3131

Demirol E, Ayoub AS (2017) Inelastic displacement ratios of SSI systems. Soil Dyn Earthq Eng, 96: 104-114.https://doi.org/10.1016/j.soildyn.2017.02.010

Dindar AA, Yalçın C, Yüksel E, Özkaynak H, Büyüköztürk O (2015) Development of earthquake energy demand spectra. EARTHQ SPECTRA, 31(3): 1667-1689.https://doi.org/10.1193/011212EQS010M

Dong HH, Han Q, Du XL, Liu JB (2020) Constant ductility inelastic displacement ratios for the design of self-centering structures with flag-shaped model subjected to pulse-type ground motions. Soil Dyn Earthq Eng, 133: 106143.https://doi.org/10.1016/j.soildyn.2020.106143

Durucan C, Dicleli M (2015) AP/VP specific inelastic displacement ratio for seismic response estimation of structures. Earthq Eng Struct D, 44(7): 1075-1097.https://doi.org/10.1002/eqe.2500

Eatherton MR, Fahnestock LA, Miller DJ (2014) Computational study of self-centering buckling-restrained braced frame seismic performance. Earthq Eng Struct D, 43(13): 1897-1914.https://doi.org/10.1002/eqe.2428

Faccioli E, Paolucci R, Rey J (2004) Displacement spectra for long periods. EARTHQ SPECTRA, 20(2): 347-376.https://doi.org/10.1193/1.1707022

Fajfar P (Ed.) (1997) Seismic Design Methodologies for the Next Generation of Codes (1st ed.). Routledge. https://doi.org/10.1201/9780203740019

Gillie JL, Rodriguez-Marek A, McDaniel C (2010) Strength reduction factors for near-fault forward-directivity ground motions. ENG STRUCT, 32(1): 273-285.https://doi.org/10.1016/j.engstruct.2009.09.014

Heresi P, Dávalos H, Miranda E (2018) Ground motion prediction model for the peak inelastic displacement of single-degree-of-freedom bilinear systems. EARTHQ SPECTRA, 34(3): 1177-1199.https://doi.org/10.1193/061517EQS118M

Iervolino I, Chioccarelli E, Baltzopoulos G (2012) Inelastic displacement ratio of near-source pulse-like ground motions. Earthq Eng Struct D, 41(15): 2351-2357.https://doi.org/10.1002/eqe.2167

Khoshnoudian F, Ahmadi E (2015) Effects of inertial soil–structure interaction on inelastic displacement ratios of SDOF oscillators subjected to pulse-like ground motions. B EARTHQ ENG, 13: 1809-1833.https://doi.org/10.1007/s10518-014-9693-y

Marquardt DW (1963) An algorithm for least-squares estimation of nonlinear parameters. J KOREAN SOC IND APP, 11(2): 431-441.https://doi.org/10.1137/0111030

Mavroeidis GP, Dong G, Papageorgiou AS (2004) Near-fault ground motions, and the response of elastic and inelastic single-degree-of-freedom (SDOF) systems. Earthq Eng Struct D, 33(9): 1023-1049.https://doi.org/10.1002/eqe.391

Miranda E (2000) Inelastic displacement ratios for structures on firm sites. J STRUCT ENG, 126(10): 1150-1159.https://doi.org/10.1061/(ASCE)0733-9445(2000)126:10(1150)

Priestley MJN (2000) Performance based seismic design. BULL N Z SOC EARTHQ, 33(3): 325-346. https://doi.org/10.5459/bnzsee.33.3.325-346

Ruiz-García J (2011) Inelastic displacement ratios for seismic assessment of structures subjected to forward-directivity near-fault ground motions. J EARTHQ ENG, 15(3): 449-468.https://doi.org/10.1080/13632469.2010.498560

Ruiz-García J, Miranda E (2004) Inelastic displacement ratios for design of structures on soft soils sites. J STRUCT

ENG, 130(12): 2051-2061.https://doi.org/10.1061/(ASCE)0733-9445(2004)130:12(2051)

Shahi SK, Baker JW (2014) An efficient algorithm to identify strong-velocity pulses in multicomponent ground motions. B SEISMOL SOC AM, 104(5): 2456-2466.https://doi.org/10.1785/0120130191

Song JK, Gavin HP (2011) Effect of hysteretic smoothness on inelastic response spectra with constant-ductility. Earthq Eng Struct D, 40(7): 771-788.https://doi.org/10.1002/eqe.1058

Song RQ, Li Y, van de Lindt JW (2014) Impact of earthquake ground motion characteristics on collapse risk of post-mainshock buildings considering aftershocks. ENG STRUCT, 81: 349-361.https://doi.org/10.1016/j.engstruct.2014.09.047

Stafford PJ, Sullivan TJ, Pennucci D (2016) Empirical correlation between inelastic and elastic spectral displacement demands. EARTHQ SPECTRA, 32(3): 1419-1448.https://doi.org/10.1193/020515EQS021M

Sucuoğlu H, Diclelil M, Nurtuğ A (1994) An analytical assessment of elastic and inelastic response spectra. CAN J CIVIL ENG, 21(3): 386-395.https://doi.org/10.1139/l94-042

Sung CH, Abrahamson NA., Huang JY (2021) Conditional ground-motion models for horizontal peak ground displacement for active crustal regions. B SEISMOL SOC AM, 111(3): 1542-1562.https://doi.org/10.1785/0120200299

Tothong P, Cornell CA (2006) An empirical ground-motion attenuation relation for inelastic spectral displacement. B SEISMOL SOC AM, 96(6): 2146-2164.https://doi.org/10.1785/0120060018

Wen WP, Zhai CH, Li S, Chang ZW, Xie LL (2014) Constant damage inelastic displacement ratios for the near-fault pulse-like ground motions. J STRUCT ENG, 59: 599-607.https://doi.org/10.1016/j.engstruct.2013.11.011

Wu YF, Li AQ, Wang H (2019) Inelastic displacement spectra for Chinese highway bridges characterized by single-degree-of-freedom bilinear systems. ADV STRUCT ENG, 22(14): 3066-3085.https://doi.org/10.1177/1369433219857845

Wu YF, Wang H, Li J, Sha B, Li AQ (2019) Inelastic Displacement Spectra and Its Utilization of DDB Design for Seismic Isolated Bridges Subjected to Near-Fault Pulse-Like Ground Motions. EARTHQ SPECTRA, 35(3): 1109-1140.https://doi.org/10.1193/033017EQS056M

Xu G, Guo T, Li AQ (2023) Self-Centering Rotational Joints for Seismic Resilient Steel Moment Resisting Frame. J STRUCT ENG, 149(2): 04022245.https://doi.org/10.1061/JSENDH.STENG-11475

Zhu RZ, Guo T, Tesfamariam S (2022) Inelastic displacement demand for non-degrading bilinear SDOF oscillators with self-centering viscous-hysteretic devices. J BUILD ENG, 48: 104010.https://doi.org/10.1016/j.jobe.2022.104010

Zhu SY, Zhang YF (2007) Seismic behaviour of self-centring braced frame buildings with reusable hysteretic damping brace. Earthq Eng Struct D, 36(10): 1329-1346.https://doi.org/10.1002/eqe.683